Preparation, Characterization, and Thermal Properties of Polystyrene-*block*-Quaternized Poly(4-vinylpyridine)/ Montmorillonite Nanocomposites

Bao-Qing Zhang, Guang-De Chen, Cai-Yuan Pan, Bin Luan, Chun-Yan Hong

Department of Polymer Science and Engineering, University of Science & Technology of China, Hefei, Anhui, 230026, People's Republic of China

Received 3 October 2005; accepted 25 March 2006
DOI 10.1002/app.24491
Published online in Wiley InterScience (www.interscience.wiley.com).

ABSTRACT: Polystyrene-*block*-poly(4-vinylpyridine) (PS-*b*-P4VP) was synthesized by two steps of reversible addition-fragmentation transfer (RAFT) polymerization of styrene (St) and 4-vinylpyridine (4VP) successively. After P4VP block was quaternized with CH_3I, PS-*b*-quaternized P4VP/montmorillonite (PS-*b*-QP4VP/MMT) nanocomposites were prepared by cationic exchange reactions of quaternary ammonium ion in the PS-*b*-QP4VP with ions in MMT. The results obtained from X-ray diffraction (XRD) and transmission electron microscopy (TEM) images demonstrate that the block copolymer/MMT nanocomposites are of intercalated and exfoliated structures, and also a small amount of silicates' layers remained in the original structure; differential scanning calorimetry (DSC) and thermal gravimetric analysis (TGA) results show that the nanocomposites displayed higher glass transition temperature (T_g) and higher thermal stability than that of the corresponding copolymers. The blending of PS-*b*-QP4VP/MMT with commercial PS makes MMT to be further separated, and the MMT was homogeneously dispersed in the polymer matrix. The enhancement of thermal stability of PS/PS-*b*-QP4VP/MMT is about 20°C in comparison with commercial PS. © 2006 Wiley Periodicals, Inc. J Appl Polym Sci 102: 1950–1958, 2006

Key words: block copolymer; clay; nanocomposite; polystyrene

INTRODUCTION

Since the report of nylon-6/clay nanocomposite by the Toyota research group,[1–3] a great number of nanocomposites based on clay and layered silicates have been extensively investigated because the starting clay materials are commercially available, and these nanocomposites exhibit markedly improved mechanical, thermal, and physical-chemistry properties, when compared with polymer/clay blends or conventional composites.[4,5]

Generally, four main strategies have been used to prepare polymer-layered silicate nanocomposites,[6] and they are exfoliation-adsorption,[7,8] *in situ* intercalative polymerization,[9–12] melt intercalation,[13,14] and template synthesis.[15] With these methods, a series of commercial vinyl polymers-layered silicate nanocomposites have been prepared. The polymers involved polystyrene (PS),[16–18] poly(methyl methacrylate) (PMMA),[6] poly(acrylamide),[19] and so on. However, only a few papers were published on the investigation of block copolymer/clay nanocomposites. For example, a commercial block copolymer, PS-*b*-poly(butadiene)-*b*-PS (SBS) was blended with a dimethyldioctadecylammonium intercalated MMT in a Brabonder at 120°C. The composites obtained showed a 5-Å increase in the interlayer spacing.[20] The copolymers include commercial SBS,[20,21] PS-*b*-PMMA,[22] and PS-*b*-polyisoprene (PS-*b*-PI).[23,24] In those nanocomposites' preparations, organically modified clays were used. Generally, they are obtained via cationic exchange reactions of clay with a long aliphatic chain ammonium salt for increasing interlayer space and modification of clay properties. For example, when sodium montmorillonite (Na-MMT) was treated with protonated dodecylamine, the interlayer spacing increased from 11.8 to 16.5 Å[17]; when it was treated with vinyl benzyl trimethyl ammonium chloride, a 5.4-Å increase of interlayer spacing was observed.[11]

Polymers were mixed with layered clay to prepare polymer/clay composites.[25,26] The polymers used included water-soluble polymers such as polyetheneoxide[27] and polydiallylamine,[28] etc. The copolymer/layered silicate hybrids were produced by intercalating poly(oxyethylene) or poly(oxypropylene)-*g*-polypropylene (POE or POP-*g*-PP) into MMT in toluene–water solution. The hybrid resembled micelles were composed of hydrophilic silicate plate as the rigid core and hydrophobic PPs in the flexible corona phase.[29] Thus, two-step procedure for synthesis of composite

Correspondence to: C.-Y. Pan (pcy@ustc.edu.cn).
Contract grant sponsor: Nano-material Science and Technology of Anhui province, China.

J_ID: Z8E Customer A_ID: 24491 Cadmus Art: APP4881 Date: 25-JULY-06 Stage: I Page: 2

materials has been developed. The first step is to mix amphiphilic block copolymers, such as poly(ethylene oxide-*b*-styrene) (PEO-*b*-PS), PEO-*b*-PMMA, PMMA-*b*-poly(methacrylic acide) and PS-*b*-P2VP, with different layered clays; the hydrophilic block in those copolymers is able to penetrate the layered inorganic structure, and the other blocks are compatible with the polymer matrix. The second step is to blend the intercalated clay with the other polymeric materials. The resulting composites with homogeneous dispersion of the layered silicates in the matrix showed better mechanical property.[30] Although the block copolymer PS-*b*-P2VP/MMT nanocomposite was investigated, detailed results of this composite were not reported, and the cationic exchange of quaternized PVP with Na^+-MMT resulted in better intercalation.[31] Generally, the block copolymer, PS-*b*-PVP is synthesized by anionic polymerization.[32] A few papers reported the synthesis of block copolymer containing PVP block by controlled radical polymerizations (CRPs).[33–35] Reversible addition-fragmentation transfer (RAFT) method has many advantages in comparison with other CRP methods.[36] Versatile monomers can be applied in the RAFT polymerization, including functional monomers. Thus, RAFT polymerization was selected to synthesize the diblock copolymers containing P4VP. In this article, we report the preparation of block copolymer PS-*b*-quaternized P4VP and its application in the synthesis of block copolymer/MMT nanocomposites; their structures and thermal properties have also been investigated.

EXPERIMENTAL

Materials

Na-MMT with ion exchange capacity of 85 meq/100 g, which was purchased from the Qingshan Chemistry Reagent Factory in Lin'an, Zhejiang, was treated by stirring MMT in deionized water for 24 h and, then, was separated by centrifugation (5000 rpm) for 0.5 h. After being dried, it was triturated and stored in a desiccator. Dimethyl formamide (DMF, Shanghai Chemical Reagent, AR, 99.5%) was distilled under reduced pressure before use. Tetrahydrofuran (THF, The First Shanghai Chemical Reagent, AR, 99%) was distilled in the presence of sodium/benzophenone. 4-Vinylpyridine (4VP, Acros Organics, CR, 95%) and styrene (St, Shanghai Chemical Reagent, CR, 99%) was distilled under reduced pressure and stored in a refrigerator. 2,2-Azobisisobutyronitrile (AIBN, The First Shanghai Chemical Reagent, CR, 98%) was purified by recrystallization from ethanol. Iodomethane (Aldrich, AR, 99.5%) was distilled prior to use. Petroleum ether, absolute diethyl ether, and chloroform ($CHCl_3$) were used without purification. Benzyl dithiobenzoate (BDTB) was prepared in 43% yield, according to the procedure reported in Ref. 24. Its ^1H NMR (300 MHz, $CDCl_3$) spectrum is shown in Figure 1(A).

Preparation of polystyrene-*block*-quaternized poly(4-vinylpyridine)

Preparation of PS

In a typical preparation procedure, AIBN (0.06 g, 0.4 mmol), BDTB (1.02 g, 4.2 mmol), St (42.93 g, 0.41 mol), and THF (10 mL) were added into a dry glass tube with a magnetic bar, followed by three freeze-vacuum-thaw cycles. The tube was sealed under vacuum and then immersed in a silicon oil bath thermostated at 110°C. After the prescribed time, the tube was cooled down to room temperature immediately. By adding the polymer solution into methanol, the polymer was precipitated and then separated by filtration. After being dried in a vacuum oven at 40°C for 24 h, the dithiobenzoate-terminated PS [PS-SC(S)Ph] was obtained (22.40 g, yield: 52%).

Preparation of PS-*b*-P4VP

AIBN (0.02 g, 0.12 mmol), PS-SC(S)SPh (M_n(NMR) = 6400, M_w/M_n = 1.06, 6.032 g, 1.04 mmol), 4VP (6.018 g, 0.057 mol), and DMF (10 mL) were successively added into a dry glass tube with a magnetic bar. After three freeze-vacuum-thaw cycles, the tube was sealed under vacuum and then the sealed tube was immersed in an oil bath at 80°C. After polymerization for 14 h, the tube was rapidly cooled down to room temperature. The copolymer was precipitated by adding the polymer solution into deionized water. After filtration, the product obtained was dissolved in $CHCl_3$ and then

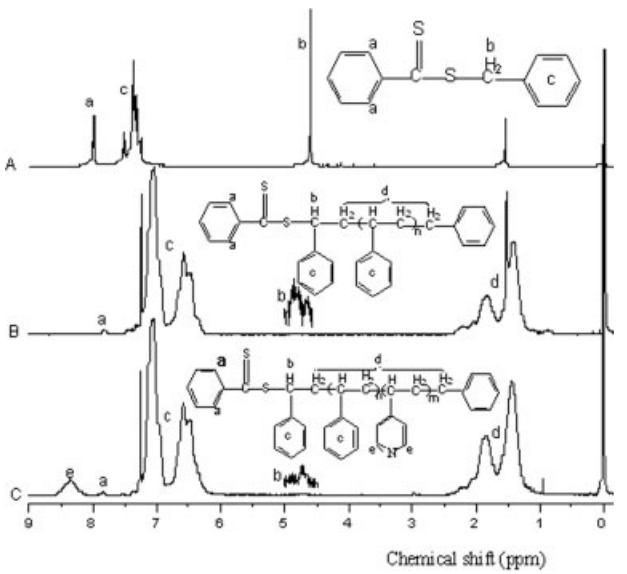

Figure 1 ^1H NMR spectra of (A) benzyl dithiobenzoate; (B) PS-SC(S)Ph_1 and (C) block copolymer (PS-*b*-P4VP)$_{1,1}$, both shown in Table I.

the solution was poured into a mixture of petroleum ether and absolute diethyl ether (1 : 1, v/v) to afford block copolymer. After being separated by filtration and being dried in a vacuum oven at 30°C for 24 h, the block copolymer polystyrene-*block*-poly(4-vinylpyridine) (PS-*b*-P4VP) was obtained.

Quaternization of 4VP in PS-*b*-P4VP

PS-*b*-P4VP (M_n = 7400, 3.409 g) was dissolved in DMF (12 mL), and then CH_3I (1.272 g, 9 mmol) was added dropwise slowly into the polymer solution at 0°C in darkness. The reaction continued at 20°C for 16 h while stirring, and then the mixture was added into excess of petroleum ether and the precipitate was filtered. Based on the decrease of characteristic band of nonquaternized 4VP units at υ = 1415 cm^{-1} in FTIR spectrum, the degree of quaternization was calculated,[35] it is ~ 95%.

Preparation of PS-*b*-QP4VP/MMT nanocomposites

A typical preparation procedure of PS-*b*-$QPVP_{1,1}$/MMT is as follows. MMT (2.14 g) was added into a solution of PS-*b*-QP4VP (equivalent ratio = 2.41 of cation exchange quantity of MMT to quaternary pyridine ammonium) in DMF prepared in the previous step, and then the reaction mixture was stirred mechanically at 80°C for 24 h. The solid was separated by filtration and was washed with DMF until no copolymer was found in the filtrate. The solid was dried in a vacuum oven at 25°C for 48 h, affording the nanocomposites (3.11 g).

Other PS-*b*-quaternized P4VP/montmorillonite (PS-*b*-QP4VP/MMT) nanocomposites were prepared with the same preparation procedure of PS-*b*-$QPVP_{1,1}$/MMT; their feed ratios and conditions are listed in Table II.

Blending of PS-*b*-QP4VP/MMT nanocomposites with PS

Commercial PS (YangZi-BASF styrenics, Nanjing, China) and various amounts of PS-*b*-QP4VP/MMT were dry-mixed and melt-blended on an internal mixer with a rotation speed of 60 rpm at 160°C for 10 min. The composites were transferred into a compression mold and hot-pressed into rectangular sheet at a temperature range of 160–170°C for 10 min at 10 MPa, and successively the mold was cooled down to room temperature while the pressure was maintained.

Characterization

^1H NMR spectra were recorded on a Bruker DMX-300 nuclear magnetic resonance (NMR) instrument with $CDCl_3$ as solvent and tetramethylsilane (TMS) as internal standard. Infrared spectra were measured on a Bruker Equinox 55 FTIR spectrometer. The molecular weight and polydispersity indexes were determined on a Waters 150C gel permeation chromatograph (GPC) equipped with ultrastyragel columns (500, 10^3, 10^4 Å) and Waters RI detector at 30°C. Monodispersed polystyrene standards were used in the calibration of molecular weights and THF was used as eluent at a flow rate of 1.0 mL/min. X-ray diffraction (XRD) spectra were collected on an X-ray diffraction instrument (X′ Pert PRO Super diffractometer, Philips) using Cu Kα radiation. The basal spacing or d_{001} spacing of the samples was calculated according to Bragg equation. The samples for transmission electron microscopy (TEM) study were prepared by placing the PS-*b*-QP4VP/MMT nanocomposite powders into epoxy resin, successively cured at 40°C for 24 h in a vacuum oven. The cured epoxy resin was microtomed into 60–90-nm-thick slices with a Reichert-Jumg Ultracut-E. Subsequently, one slice was placed on a 100-mesh copper net for TEM observation on a JEOL-200FX with an acceleration voltage of 100 kV. Differential scanning calorimetry (DSC) measurements were implemented on a Mettler Toledo DSC-822^e at the heating rate of 20°C/min from 20 to 220°C at the nitrogen flow rate of 60.0 mL/min. The glass transition temperature (T_g) of PS-*b*-P4VP was based on the second scanning. Thermal gravimetric analysis (TGA) was carried out on a Shimadzu DT-50 Thermogravimetric Analyzer at a heating rate of 10°C/min from room temperature to 800°C at nitrogen flow rate of 20.0 mL/min.

RESULTS AND DISCUSSION

Preparation of quaternized poly(4-vinyl pyridine)-*b*-PS

For preparation of QPVP-*b*-PS/MMT nanocomposites by cation exchange with MMT, the first step is preparation of diblock copolymers, (PVP-*b*-PS)s with different molecular weights, and they were synthesized by RAFT polymerization according to Scheme 1. The synthetic conditions and the results are listed in Table I.

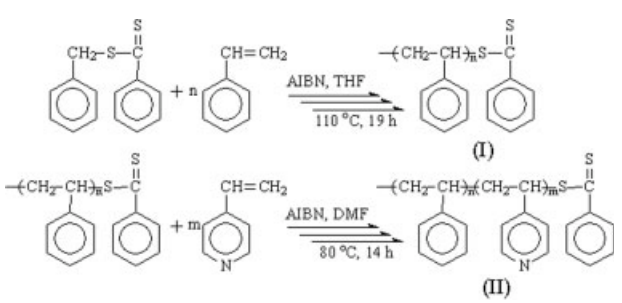

Scheme 1 Preparation of diblock copolymer, PS-*b*-P4VP.

TABLE I
The Conditions and Results of RAFT Block Copolymerization of 4VP Using PS-SC(S)Ph as RAFT Agent

Polymer	Feed molar ratio[a] AIBN : B : M	T (°C)	t (h)	Yield (%)	M_n[c] (NMR)	St : 4VP (molar ratio)
PS-SC(S)Ph$_1$	1 : 10.5 : 1025	110	19	52	6400	
(PS-*b*-P4VP)$_{1,1}$[b]	1 : 8.6 : 522	80	14	11	7400	6.4 : 1
(PS-*b*-P4VP)$_{1,2}$[b]	1 : 14.7 : 890	80	24	56	11500	1.3 : 1
PS-SC(S)Ph$_2$	1 : 9.8 : 2058	110	22	54	13600	
(PS-*b*-P4VP)$_2$[b]	1 : 4.9 : 267	80	36	38	18400	2.8 : 1
PS-SC(S)Ph$_3$	1 : 10.1 : 5263	110	22	60	33600	
(PS-*b*-P4VP)$_3$[b]	1 : 2.8 : 237	80	36	35	38400	7 : 1
PS-SC(S)Ph$_4$	1 : 9.9 : 8761	110	22	58	56400	
(PS-*b*-P4VP)$_4$[b]	1 : 2.5 : 268	80	36	33	62400	9.4 : 1

[a] For polymerization of St, B is BDTB; M is St; for block copolymerization of 4VP, B is PS-SC(S)Ph, M is 4VP.
[b] GPC curves of PS-*b*-P4VP were not measured because the block copolymers are not dissolved in THF.
[c] Number-average molecular weight, M_n (NMR) was calculated based on ^{1}H NMR data.

The macro RAFT agents PS-SC(S)SPhs were prepared by RAFT polymerization of St at 110°C, using AIBN as initiator and BDTB as chain transfer agent. The structure of the polymers obtained was confirmed by their ^{1}H NMR spectra. Figure 1(B) represents a typical ^{1}H NMR spectrum of PS-SC(S)Ph$_1$ shown in Table I. Except the signals of phenyl protons of St units at 6.2–7.4 ppm and the signals of methylene and methine protons in the polymer backbone at 1.0–2.4 ppm, a signal at $\delta = 7.84$ ppm belongs to the phenyl protons ortho to the dithiobenzoate group. Based on the integration ratio of the signals at $\delta = 6.20$–6.80 ppm to that at $\delta = 7.84$ ppm, the molecular weight of PS-SC(S)SPh obtained can be calculated, and it agrees with $M_{n,GPC}$ obtained from GPC measurement. The polydispersity is narrow (below 1.2). For example, M_n (NMR) of PS-SC(S)SPh$_1$ was 6400 and GPC result was 5800. The polydispersity index was 1.08.

Block copolymerization of 4VP was carried out in DMF, using AIBN as initiator and PS-SC(S)Ph as RAFT agent. By varying feed molar ratio of 4VP to PS-SC(S)Ph, the block copolymers with different molecular weights of P4VP block (for example, $M_n = 7400$, $M_{n,vp}$ of P4VP = 1000; $M_n = 11{,}500$, $M_{n,vp} = 5100$) were obtained (Table I). A typical ^{1}HNMR spectrum of the block copolymer (PS-*b*-P4VP)$_{1.1}$ (Table I) is shown in Figure 1(C). In comparison with Figure 1(B), Figure 1(C) shows the signals of *meta*-protons of pyridine ring at $\delta = 8.20$–8.60 ppm (e) and two phenyl protons ortho to dithiobenzoate group at $\delta = 7.84$ ppm (a). The molecular weight of P4VP segment in copolymer can be calculated based on the integration ratio of signals at 8.20–8.60 to that at 6.20–6.80 ppm. The compositions of block copolymers were calculated and the results are listed in Table I.

Preparation and structure of PS-*b*-QP4VP/MMT nanocomposites

The cationic exchange of PS-*b*-QP4VP with cations in MMT was carried out in DMF solution and the block copolymer/MMT nanocomposites were obtained. The conditions and results are listed in Table II.

TABLE II
Preparation Conditions and Results of PS-*b*-QP4VP/MMT Nanocomposites

Composite	Polymer[a]	Quaternization[b] P (g)	Quaternization[b] CH_3I (g)	Quaternization[b] DMF (mL)	MMT[c] (g)	Yield[d] (%)	Polymer content (wt %)
PS-*b*-QPVP$_{1,1}$/MMT	(PS-*b*-P4VP)$_{1,1}$	3.409	1.272	8	2.14	35	31
PS-*b*-QPVP$_{1,2}$/MMT	(PS-*b*-P4VP)$_{1,2}$	2.786	1.818	10	2.54	41	36
PS-*b*-QPVP$_2$/MMT	(PS-*b*-P4VP)$_2$	1.157	0.786	12	1.56	47	26
PS-*b*-QPVP$_3$/MMT	(PS-*b*-P4VP)$_3$	2.462	0.984	12	1.93	12	13
PS-*b*-QPVP$_4$/MMT	(PS-*b*-P4VP)$_4$	3.059	1.602	15	1.96	4	6

[a] Block copolymers are the same with that in Table 1.
[b] Quaternization reaction conditions: temperature: 35°C; reaction time: 8 h.
[c] The preparation conditions of PS-*b*-QP4VP/MMT nanocomposites: temperature: 80°C; reaction time: 24 h.
[d] Yield (%) = weight of the polymer intercalated in nanocomposites/weight of PS-*b*-P4VP used in the cation exchange.

A basic evidence of the polymer intercalation into MMT is the weight increase of polymer/MMT composites obtained from the exchange reaction solution (Table II). The intercalation can be further confirmed by their FTIR spectra. A typical FTIR spectrum of the (PS-*b*-QP4VP)$_{1.1}$/MMT sample, in Table II, is shown in Figure 2(b). In comparison with FTIR spectrum of MMT in Figure 2(a), Figure 2(b) shows a series of characteristic bands of PS-*b*-QP4VP: aromatic C—H stretching vibration bands at around υ = 3025 cm^{-1}, the C—H stretching bands of methylene and methine groups in the backbone at 3000–2840 cm^{-1}, and the combination and overtone bands at 1950–1730 cm^{-1}; the out of plane C—H bending vibration bands at 700 cm^{-1} and the characteristic bands of quaternized 4VP units at υ = 1639 cm^{-1} and nonquaternized 4VP units at 1415 cm^{-1}.[35] The Si—O vibration at $\sim$ 1040 cm^{-1} is from MMT.[37]

For characterizing the structure of the nanocomposites, their XRD measurements were carried out and their images are shown in Figure 3. Studying the effects of PS chain length on the intercalation should be interesting. Different compositions of block copolymers were used in the intercalation reaction with MMT. With the same preparation conditions of nanocomposites, the contents of copolymers in the nanocomposites obtained are listed in Table II. We can find in this table that with the molecular weight increase of PS block, the contents of polymers intercalated in MMT decreased. This phenomenon can be further confirmed by their XRD patterns in Figure 3. With the molecular weight decrease of PS block from 56,400 to 33,600 and to 6400, the diffraction peaks are shifted from 2θ = 6.62°(MMT, d_{001} = 1.34 nm) to 6.08° (d_{001} = 1.48 nm), to 5.98° (1.50 nm) and to 5.70° (1.55 nm) gradually. This demonstrates that the larger the molecular weights of PS segment, the bigger the resistance to the intercalation of block copolymers. This might be reasonable; the longer the chain length of PS block, the higher the resistance to the driving force of cationic exchange reaction. Hydrophilic reduction of the block copolymers with the increase of PS chain length may be another reason for the decrease of polymer content in the nanocomposites.

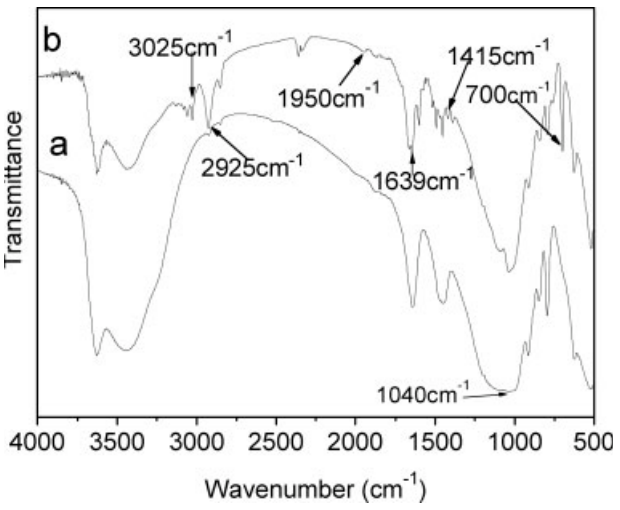

Figure 2 FTIR spectra of (a) MMT and (b) (PS-*b*-QP4VP)$_{1,1}$/MMT nanocomposite (Table I).

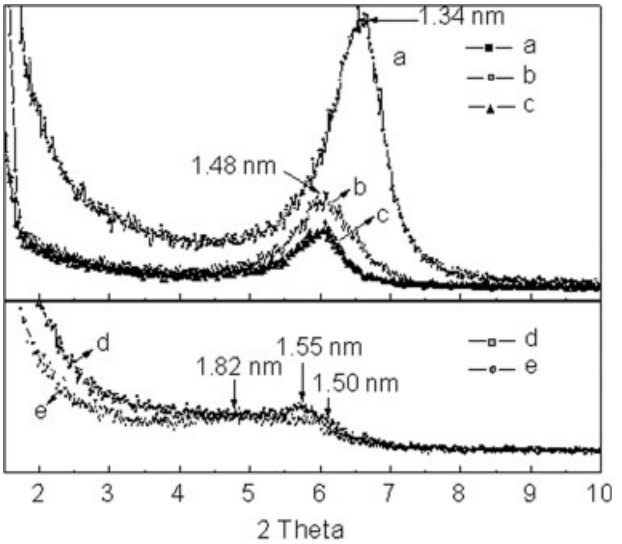

Figure 3 XRD patterns of MMT (a); (PS-*b*-QP4VP)$_4$/MMT composite (Table II) prepared from block copolymer (PS-*b*-QP4VP)$_4$, with PS block (M_n = 56,400) and P4VP block of M_n 6000 (b); (PS-*b*-QP4VP)$_3$/MMT composite prepared from (PS-*b*-QP4VP)$_3$, with PS of M_n 33,600 and P4VP of M_n 4800 (c); (PS-*b*-QP4VP)$_{1,1}$/MMT composite prepared from (PS-*b*-QP4VP)$_{1,1}$, with PS of M_n 6400 and P4VP of M_n 1000 (d); (PS-*b*-QP4VP)$_{1,2}$/MMT composite prepared from (PS-*b*-QP4VP)$_{1,1}$, with PS of M_n 6400 and P4VP of M_n 5100 (e).

We also studied the effect of polymerization degree ratios of PS to P4VP in the diblock copolymers on the intercalation. The (PS-*b*-QP4VP$_{1.1}$) (6.4 : 1) and (PS-*b*-QP4VP$_{1.2}$) (1.3 : 1) were used in the intercalation reactions to afford two nanocomposites (PS-*b*-QP4VP)$_{1.1}$/MMT and (PS-*b*-QP4VP)$_{1.2}$/MMT, respectively. Their XRD patterns [Figs. 3(d) and 3(e)] and the weight increase [(PS-*b*-QP4VP)$_{1.1}$/MMT and (PS-*b*-QP4VP)$_{1.2}$/MMT in Table II] reveal that the ratio increase of P4VP to PS blocks will be favorable to the intercalation, probably because of stronger driving force of cationic exchange reaction.

To further characterize the structure of block copolymer/MMT nanocomposites obtained, their TEM images were taken. Figure 4 shows the TEM images of the nanocomposites (PS-*b*-QP4VP)$_{1.1}$/MMT and (PS-*b*-QP4VP)$_{1.2}$/MMT. Obviously the MMT layers (black line) are separated by block copolymers (white region) in Figures 4(a) and 4(b). For examining the accurate structure of polymer/MMT nanocomposites, high resolution TEM images were taken as shown in Figures 4(c) and 4(d). We can see that some parts of the nanocomposite are intercalated by

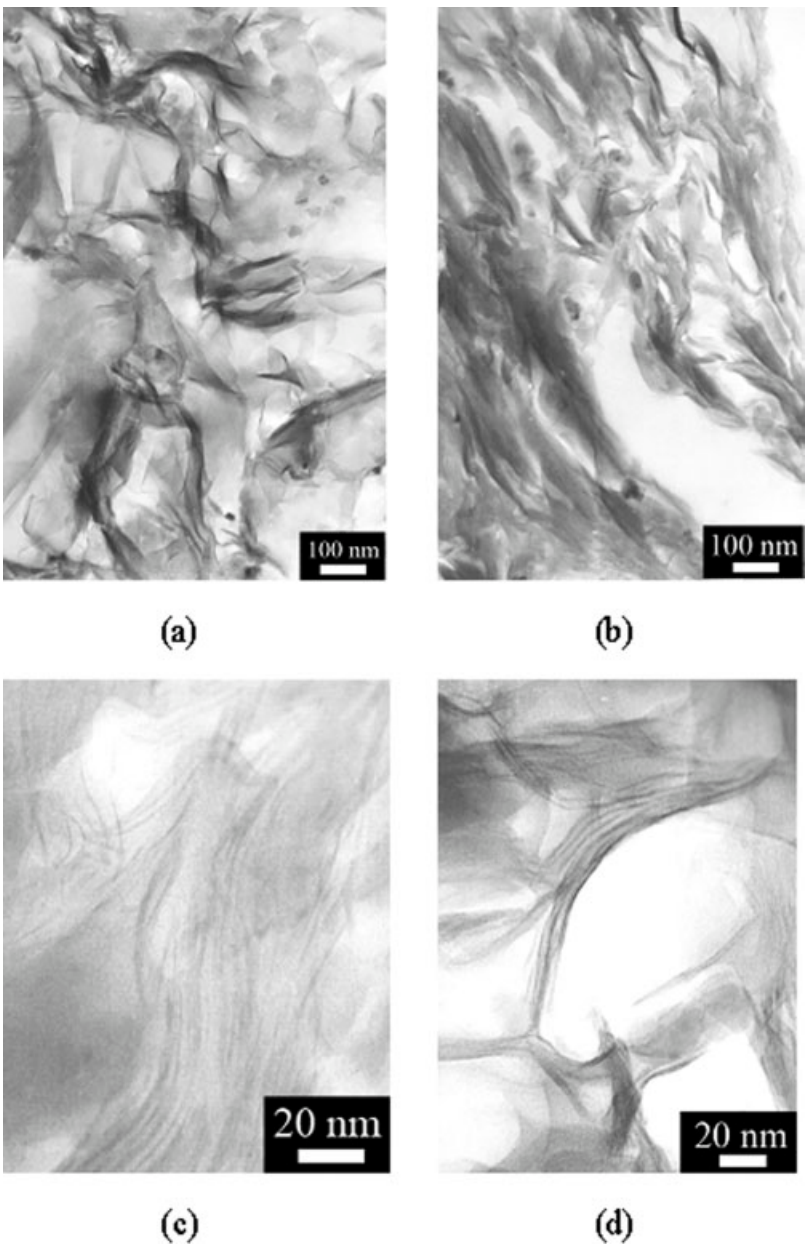

Figure 4 TEM images of (PS-*b*-QP4VP)$_{1.1}$/MMT nanocomposite, with magnification ×50,000 (a), ×150,000 (c), and (PS-*b*-QP4VP)$_{1.2}$/MMT nanocomposite, with magnification ×50,000 (b), ×200,000 (d).

the copolymer with the interlayer spacing ranging from 2 to 7 nm, although a small amount of silicate layers were not intercalated by block copolymers. These results match well with their XRD patterns in Figure 4.

It is well known that the interaction of block copolymer in MMT will affect the thermal behavior of block copolymer. Thus, the DSC curves of the block copolymer PS-*b*-P4VP$_{1.1}$, (PS-*b*-QP4VP)$_{1,1}$/MMT and (PS-*b*-QP4VP)$_{1,2}$/MMT nanocomposites were measured, and they are shown in Figure 5. The pure PS-*b*-P4VP$_{1.1}$ copolymer exhibits two glass transition temperatures (T_gs): one T_g of PS is 100.8°C, the other is the T_g of P4VP at 130.9°C [Fig. 5(a)]. In the DSC curves of (PS-*b*-QP4VP)$_{1,1}$/MMT and (PS-*b*-QP4VP)$_{1,2}$/MMT nanocomposites in Figures 5(b) and 5(c), only T_gs of PS block appeared at 110.1°C and 113.3°C, respectively, and T_g of P4VP block disappeared. This phenomenon can be interpreted as follows. The motion of PS chains inserted in the interlayer spacing between MMT layers is retarded, resulting in T_g increase of PS. The quaternary pyridine groups of QP4VP blocks are interacted with the anionic charge of the silicate layers; thus, the motion of QP4VP chains is highly restricted, or the QP4VP domains near the silicate layers are so small, resulting in the

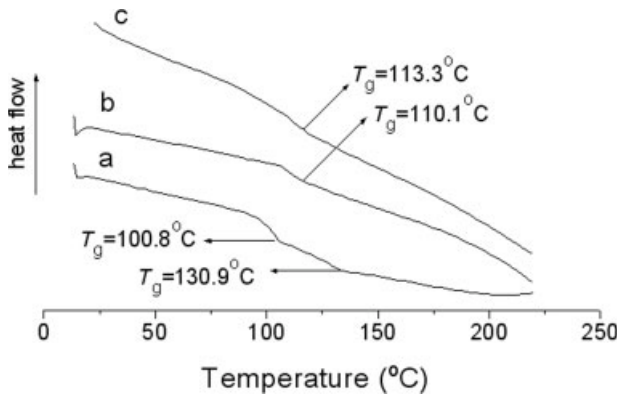

Figure 5 DSC heating curves of (a) PS-*b*-P4VP, (b) (PS-*b*-QP4VP)$_{1.1}$/MMT nanocomposite shown in Table II, and (c) (PS-*b*-QP4VP)$_{1.2}$/MMT nanocomposite (Table II).

invisibility of its T_g. In comparison with the T_g (110.1°C) of (PS-*b*-QP4VP)$_{1,1}$/MMT composite, the higher content of Q4PVP in (PS-*b*-QP4VP)$_{1,2}$ leads to higher T_g (113.3°C) of PS, the higher restriction of PS chain motion is due to the stronger interaction between Q4VP chain and MMT platelets.

Thermal properties of (PS-*b*-QP4VP)/MMT composites

One of highly interesting properties for the polymer/layered silicate nanocomposites is their increased thermal stability, which was assessed by TGA. Figure 6 shows the TGA and DTG curves of (PS-*b*-QP4VP)$_{1,1}$/MMT and (PS-*b*-QP4VP)$_{1,2}$/MMT nanocomposites. For comparison, the TGA and DTG curves for a mixture of block copolymer and MMT (weight ratio of PS-*b*-P4VP to MMT is 1 : 1) were also measured, and they are shown in Figures 6(A) and 6(B), respectively. All curves in Figure 6(A) show a little weight loss below 200°C, probably due to evaporation of the water absorbed on MMT. And the thermal degradation temperatures of the two nanocomposites are 372 and 371°C respectively, 30°C higher than that (341°C) of the block copolymer in the blends of the copolymer and MMT. In the DTG curves of Figure 6(B), we could observe one peak of weight loss, and the maximum temperatures of peaks for the blend of copolymer and MMT, (PS-*b*-QP4VP)$_{1,1}$/MMT, and (PS-*b*-QP4VP)$_{1,2}$/MMT nanocomposites are 379, 412, and 408°C respectively. The thermal stability of the nanocomposites is also 30°C higher than that of the composite prepared by simple blending. This may be ascribed to the inhomogeneous distribution of MMT in the polymer matrix due to less intercalation of block copolymer into MMT during blending. At 500°C, the weight loss in the blend of copolymer and MMT, (PS-*b*-QP4VP)$_{1,1}$/MMT, and (PS-*b*-QP4VP)$_{1,2}$/MMT nanocomposites are 51%, 33%, and 29%, respectively, similar to the contents (50%, 36%, 31%) of block copolymer in their composites.

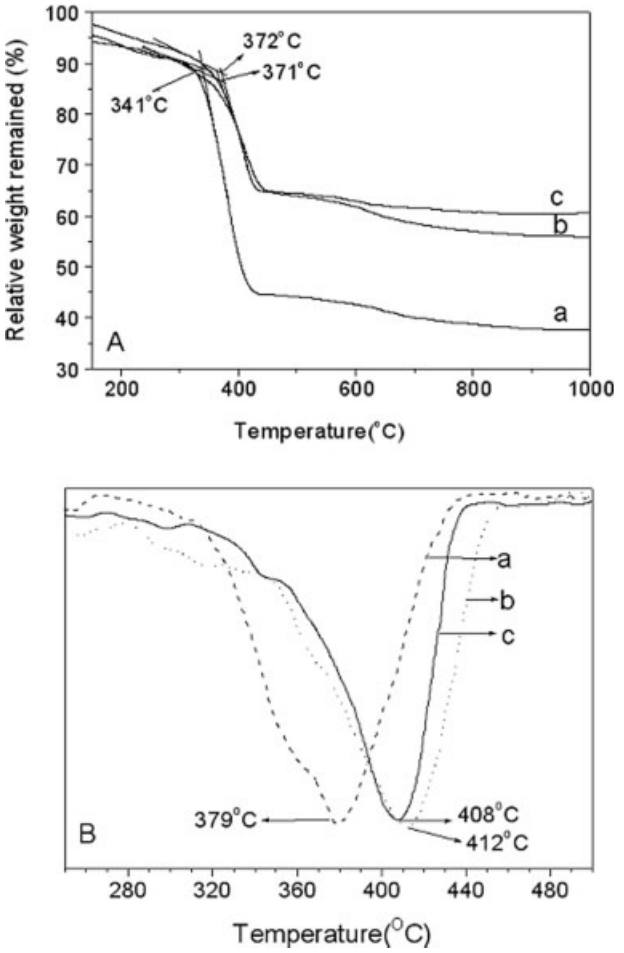

Figure 6 TGA (A) and DTG (B) curves of (a) the mixture of PS-*b*-P4VP and MMT, (b) (PS-*b*-QP4VP)$_{1.1}$/MMT nanocomposite and (c) (PS-*b*-QP4VP)$_{1.2}$/MMT nanocomposite shown in Table II.

Preparation and characterization of PS/PS-*b*-QP4VP/MMT nanocomposites

For natural MMT, its hydrophilic property results in poor compatibility with organic materials, so that uniform dispersion of layered silicates in a polymer

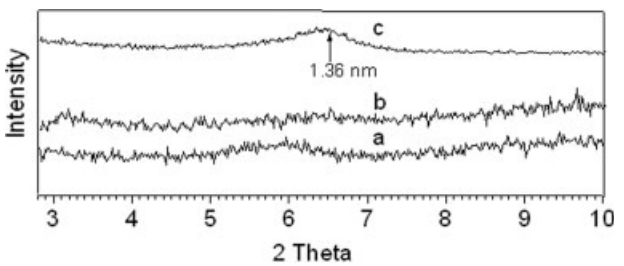

Figure 7 XRD patterns of the composites prepared by blending commercial PS and PS-*b*-Q4VP/MMT composites; (a) the composite containing 5 wt % MMT prepared from (PS-*b*-QP4VP)$_{1.2}$/MMT; (b) the composite containing 3 wt % MMT prepared from (PS-*b*-QP4VP)$_{1.2}$/MMT; (c) the composite with 5 wt % MMT from (PS-*b*-QP4VP)$_3$/MMT.

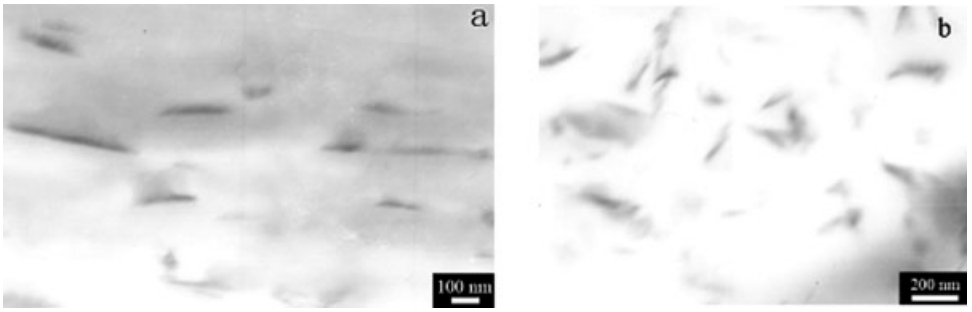

Figure 8 TEM images of the composites with 3 wt % MMT (a) and 5 wt % MMT (b) prepared from blending pure PS with (PS-*b*-PQ4VP)$_{1,2}$/MMT.

matrix is very difficult. After intercalation of diblock copolymers, PS-*b*-QP4VP, the compatibility of PS-*b*-QP4VP/MMT with polymers should be improved greatly. Therefore, the compatibility of the intercalated MMT with pure PS was studied.

Blending PS-*b*-QP4VP/MMT with commercial PS was performed in an internal mixer. The contents of MMT in the nanocomposites produced were 3 wt % and 5 wt %. Their XRD patterns are shown in Figure 7. The reflection peaks of MMT in Figures 7(a) and 7(b) are almost invisible, indicating the formation of almost exfoliate structure in the nanocomposites. When the molecular weight of PS block in the block copolymer increased to 33,600, the reflection peak of MMT is almost the same with that of the starting MMT [Fig. 7(c)]. This demonstrates that most of MMT was not intercalated by diblock copolymers, which is consistent with the result in Figure 3 and also with the less content of block copolymer in (PS-*b*-QP4VP)$_3$/MMT listed in Table II. The TEM images of PS/(PS-*b*-QP4VP)$_{1,2}$/MMT with 3 wt % and 5 wt % MMT are shown in Figures 8(a) and 8(b), respectively. The homogeneous distribution of silicate platelets in the polymer matrix can be observed. The partially exfoliated MMT platelets in the PS-*b*-QP4VP/MMT composites were further separated during the blending.

Thermal stability of PS/PS-*b*-QP4VP/MMT nanocomposites

Thermal stability of the blended composites made from PS and PS-*b*-QP4VP/MMT was studied by TGA method. Figure 9 shows the TGA and DTG curves of commercial PS, PS/(PS-*b*-QP4VP)$_{1,2}$/MMT, and PS/(PS-*b*-QP4VP)$_2$/MMT. In comparison with the onset decomposition temperature of commercial PS, the temperatures for the blended composites in Figure 9(A) are shifted to a higher temperature range, indicating the enhancement of the thermal stability of the blended composites. Compared with the maximum decomposition temperature (396°C) of commercial PS, the temperatures of the blended composites enhanced to 416°C and 414°C respectively, [Fig. 9(B)]. The thermal stability improvement of the composites may be ascribed to their structures and the restricted thermal motion of the PS in the gallery,[38] and the interaction between PS and PS-*b*-QPVP/MMT may be another

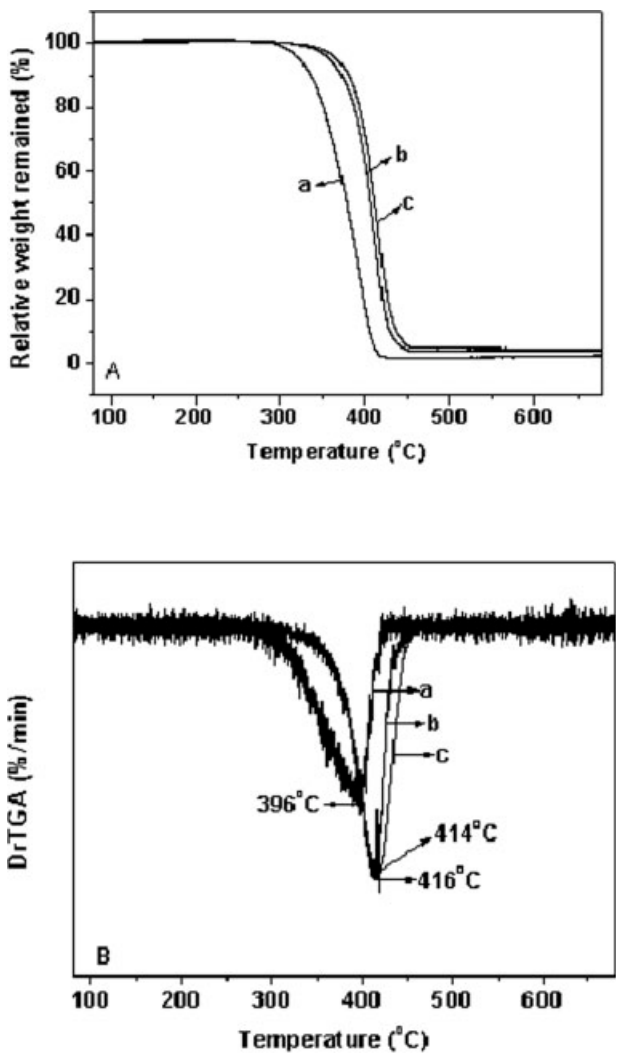

Figure 9 TGA (A) and DTG (B) curves of (a) commercial PS; (b) the composite of commercial PS blended with 5 wt % (PS-*b*-QP4VP)$_2$/MMT; and (c) the composite of commercial PS blended with 5 wt % (PS-*b*-QP4VP)$_{1,2}$/MMT.

reason. The slight enhancement of thermal stability for the PS/(PS-*b*-QP4VP)$_{1,2}$/MMT than that for PS/(PS-*b*-QP4VP)$_2$/MMT may be due to the increased thermal insulation effect of MMT, because layered silicates in the former composites dispersed more homogeneously.

CONCLUSIONS

Amphiphilic diblock copolymers, PS-*b*-QP4VPs have been successfully prepared by RAFT polymerization of 4VP using AIBN as initiator, PS-SC(S)Ph as RAFT agent, and following quaternization reaction of P4VP with CH_3I. Direct cationic exchange of ammonium ions in the block copolymers with cations in MMT produced PS-*b*-QP4VP/MMT nanocomposites containing different contents of block copolymers. The XRD results and TEM images show that the nanocomposites have exfoliated and intercalated structures, as well as other intermediate organizations. With the molecular weight increase of PS blocks from $M_n = 6400$ to 13,600 to 33,600 and to 56,400, the weight contents of block copolymers in the nanocomposites decreased from 36% to 26% to 13% to 6%, indicating that the long chain length of PS block is a resistance to the driving force of cationic exchange reactions between quaternary pyridine cations and cations in MMT. The T_gs of PS and P4VP blocks in the block copolymers are 100.8°C and 130.9°C, respectively. The DSC curves of the nanocomposites show only one T_g of PS block, and T_g of P4VP block is invisible. The T_gs (110°C and 113°C) of PS in the two nanocomposites are 10°C higher than that of PS in the block copolymers. The thermal stability of block copolymer in the nanocomposites is 30°C higher than that in the blended composites composed of block copolymers and MMT. After blending PS-*b*-QP4VP/MMT nanocomposites with commercial PS, MMT was further exfoliated and dispersed in the polymer matrix homogeneously. Its thermal stability is also improved.

References

1. Usuki, A.; Kawasumi, M.; Kojima, Y.; Okada, A.; Kurauchi, T.; Kamigaito, O. J Mater Res 1993, 8, 1174.
2. Usuki, A.; Kojima, Y.; Kawasumi, M.; Okada, A.; Fukushima, Y.; Kurauchi, T.; Kamigaito, O. J Mater Res 1993, 8, 1179.
3. Kojima, Y.; Usuki, A.; Kawasumi, M.; Okada, A.; Fukushima, Y.; Kurauchi, T.; Kamigaito, O. J Mater Res 1993, 8, 1185.
4. Alexandre, M.; Dubois, P. Mater Sci Eng R Rep 2000, 28, 1.
5. Biswas, M.; Ray, S. S. Adv Polym Sci 2001, 155, 167.
6. Koo, C. M.; Ham, H. T.; Kim, S. O.; Wang, K. H.; Chung, I. J.; Kim, D. C.; Zin, W. C. Macromolecules 2002, 35, 5116.
7. Lee, D. C.; Jang, L. W. J Appl Polym Sci 1996, 61, 1117.
8. Oriakhi, C. O.; Zhang, X. R.; Lerner, M. M. Appl Clay Sci 1999, 15, 109.
9. Zhao, H. Y.; Shipp, D. A. Chem Mater 2003, 15, 2693.
10. Reichert, P.; Kressler, J.; Thomann, R.; Mulhaupt, R.; Stoppelmann, G. Acta Polym 1998, 49, 116.
11. Akelah, A.; Moet, A. J Mater Sci 1996, 31, 3589.
12. Doh, J. G.; Cho, I. Polym Bull 1998, 41, 511.
13. Vaia, R. A.; Giannelis, E. P. Macromolecules 1997, 30, 8000.
14. Kato, M.; Usuki, A.; Okada, A. J Appl Polym Sci 1997, 66, 1781.
15. Carrado, K. A.; Xu, L. Q. Chem Mater 1998, 10, 1440.
16. Zhu, J.; Start, P.; Mauritz, K. A.; Wilkie, C. A. J Polym Sci Part A: Polym Chem 2002, 40, 1498.
17. Fu, X.; Qutubuddin, S. Polymer 2001, 42, 807.
18. Hasegawa, N.; Okamoto, H.; Kawasumi, M.; Usuki A. J Appl Polym Sci 1999, 74, 3359.
19. Asselman, T.; Garnier, G. Colloids Surf A 2000, 170, 79.
20. Laus, M.; Francescangeli, O.; Sandrolini, F. J Mater Res 1997, 12, 3134.
21. Ha, Y. H.; Thomas, E. L. Macromolecules 2002, 35, 4419.
22. Limary, R.; Swinnea, S.; Green, P. F. Macromolecules 2000, 33, 5227.
23. Ren, J. X.; Silva, A. S.; Krishnamoorti, R. Macromolecules 2000, 33, 3739.
24. Ren, J.; Krishnamoorti, R. Macromolecules 2003, 36, 4443.
25. Aranda, P.; Ruizhitzky, E. Chem Mater 1992, 4, 1395.
26. Wu, J. H.; Lerner, M. M. Chem Mater 1993, 5, 853.
27. Vaia, R. A.; Vasudevan, S.; Krawiec, W.; Scanlon, L. G.; Giannelis, E. P. Adv Mater 1995, 7, 154.
28. Kleinfeld, E. R.; Ferguson, G. S. Science 1994, 265, 370.
29. Lin, J. J.; Hsu, Y. C.; Chou, C. C. Langmuir 2003, 19, 5184.
30. Fischer, H. R.; Gielgens, L. H.; Koster, T. P. M. Acta Polym 1999, 50, 122.
31. Toomey, R.; Mays, J.; Tirrell, M. Macromolecules 2004, 37, 905.
32. Choi, M.; Chung, B.; Chun, B.; Chang, T. Macromol Res 2004, 12, 127.
33. Ohno, K.; Ejaz, M.; Fukuda, T.; Miyamoto, T.; Shimizu, Y. Macromol Chem Phys 1998, 199, 291.
34. Xia, J. H.; Zhang, X.; Matyjaszewski, K. Macromolecules 1999, 32, 3531.
35. Lysenko, E. A.; Bronich, T. K.; Slonkina, E. V.; Eisenberg, A.; Kabanov, V. A.; Kabonov, A. V. Macromolecules 2002, 35, 6344.
36. Pyun, J.; Matyjaszewski, K. Chem Mater 2001, 13, 3436.
37. Bai, S. L.; Wang, Z. Q.; Zhang, X. Langmuir 2004, 20, 11828.
38. Gilman, J. W. Appl Clay Sci 1999, 15, 31.